Astron. Astrophys. 346, 1011–1019 (1999)

ASTRONOMY AND ASTROPHYSICS

Dynamics of particles in Saturn's E ring: effects of charge variations and the plasma drag force

Valery V. Dikarev

Astronomical Institute, St. Petersburg University, Stary Peterhof, 198904 St. Petersburg, Russia (valery@astro.spbu.ru)

Received 20 November 1998 / Accepted 30 March 1999

Abstract. Dynamics of the E ring dust grains in Saturn's magnetosphere are investigated. Apart from the solar radiation pressure and the planetary oblateness, the Lorentz force due to variable charge and the plasma drag are taken into account.

The Lorentz force is considered for the grain's charge which does not depend on time explicitly but is a function of the grain's distance from the planet. Under this assumption and neglecting small orbital inclinations the Lorentz force leaves the eccentricity unaltered but causes precession or regression of the orbit with the rate determined by the charging model. It is shown that the orbital evolution of the grains having a variable charge does not differ qualitatively from that of the grains with a constant charge.

The action of the plasma drag is investigated analytically in the approximation of small eccentricities and zero inclinations. The direct drag due to the fraction of the heavy ions (O^+, OH^+) is found to be the main drag force in the inner magnetosphere of Saturn. The plasma drag alone changes the semimajor axis. The rate of the semimajor axis growth due to the plasma drag is large enough to allow the submicron-sized grains ejected from Enceladus to survive against recollision with the parent satellite. When combined with the radiation pressure, the plasma drag also introduces the trend in the oscillating eccentricity which leads to the growth of the eccentricity of the E ring grain orbits.

Key words: methods: analytical – celestial mechanics, stellar dynamics – meteors, meteoroids – planets and satellites: general – planets and satellites: individual: Enceladus

1. Introduction

The E ring is the dust complex extending from ~ 3 to 8 planetary radii in Saturn's equatorial plane. It is composed of grains having a narrow size distribution centered in the interval from 3 to $0.3\ \mu$m (Nicholson et al. 1996). The peak of the ring's brightness is located close to the orbit of Enceladus, which strongly suggests that this satellite serves as the source of the E ring dust.

The tiny grains immersed in Saturn's magnetosphere are subject to many perturbations. As long as a grain moves in the ambient plasma, it collects electrostatic charge which rises the Lorentz force in the planetary magnetic field. The interaction with the plasma itself invokes the drag force because of the grain's velocity relative to the bulk of plasma. The solar radiation pressure and the planetary oblateness further complicate the dynamics.

Previous theoretical studies reveal that many features of the E ring can be explained provided the particle dynamics are determined by the combined perturbations due to the radiation pressure, planetary oblateness and the Lorentz force. Horányi et al. (1992) use the sophisticated charging model and predict nearly constant grain's potential throughout the ring's extent. They argue that only micron-sized grains attain orbits with large eccentricities and hence cover the broad range of radial distances. Hamilton & Krivov (1996) develop the analytical theory for the circumplanetary dust dynamics with an application, among others, to Saturn's E ring. Describing the Lorentz force they restrict the theory to the constant charge and find an integral of the planar motion which accounts for the radiation pressure, planetary oblateness, electromagnetism and the solar gravity. For the planar case they consider, this permits them to describe in detail the character of motion in the form of phase portraits.

However, the mechanism of dust charging in space is full of large uncertainties. Several charging models developed by Horányi et al. (1992), Morfill et al. (1993) and Jurac et al. (1995) predict different potentials for the E ring grains. Most potentials do not keep constant when the grain's orbit is eccentric, and the ambient plasma parameters vary periodically. The survival of highly eccentric orbits when the charge varies is crucial for the present model of the E ring. And *vice versa* if the ring's model is correct, the choice between the charging models can be done on the base of particle dynamics.

Most recently Dikarev & Krivov (1998) added the plasma drag effect to the particle dynamics. Using numerical integrations of the Newtonian equations of the motion, they showed that the growth of the semimajor axis allows the eccentric orbits of the grains to cover the full radial extension of the E ring, at the same time introducing new kinds of the orbital behaviour.

This paper extends the existing models for the circumplanetary dust dynamics in two directions. First, the analytical theory (Hamilton & Krivov 1996) is generalized to account for the variable charge in a reasonable approximation. The consistency of

Send offprint requests to: V.V. Dikarev

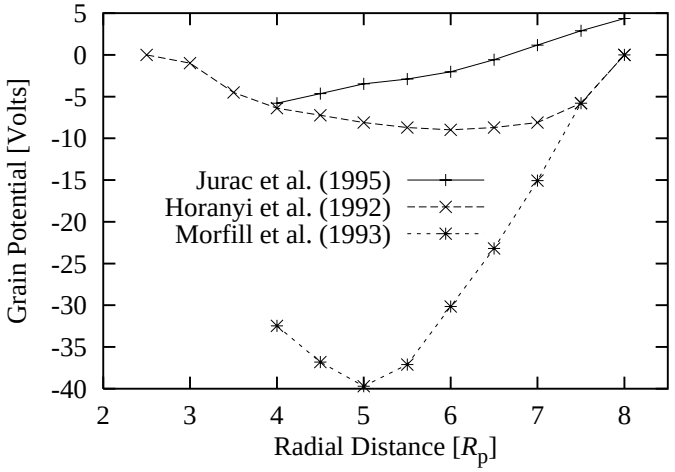

Fig. 1. The grain potentials versus planetocentric distance.

several charging models with the existence of a broad dust complex in view of the particle dynamics is then examined (Sect. 2). Second, the action of the plasma drag is investigated in more detail than in our previous dynamical model (Dikarev & Krivov 1998). In the limit of small eccentricities and zero inclinations, an analytical description of the motion is developed (Sect. 3). Conclusions are made in Sect. 4.

2. The charge variations

2.1. Charge and its variability

The E ring dust is immersed deeply in Saturn's magnetosphere which is characterized by a strong magnetic field (Acuña et al. 1983) and dense plasma (see Richardson 1995 and references therein). As long as the grains move in the ambient plasma, they collect charge which raises the Lorentz force in the planetary magnetic field. To account for the Lorentz force properly, one needs to know the grain's charge as well as its variations. In practice the electric potential of the grain φ is evaluated. The charge of the grain of radius s is then calculated using the equation $300\,q = \varphi s$ (q and s are in CGS units, φ in Volts).

Evaluation of a grain's potential is not an easy task. It requires knowledge of the physical, chemical and geometrical properties of the grain, as well as the ambient plasma parameters and the grain's velocity relative to the bulk of plasma. E ring grains' potentials were calculated in a number of papers (Fig. 1). We have selected some of them for comparison of the relevant particle dynamics (Jurac et al. 1995, their Fig. 6-b; Horányi et al. 1992, their Fig. 1, curve for secondary electron emission parameters $E_{\rm m} = 500$ eV, $\delta_{\rm m} = 1.0$; Morfill et al. 1993, their Fig. 4, curve for $E_{\rm m} = 1000$ eV, $\delta_{\rm m} = 1.0$). Also discussed is the constant charge -5.6 V since it is close to the "best guess" charge of Horányi et al. (1992).

The grain's potential is usually found by solving the current balance equation

$$\sum_i j_i(\varphi) = 0, \qquad (1)$$

where $j_i(\varphi)$ are e.g. electron and ion fluxes incident on a grain, photoelectron current, etc. In so doing, circular equatorial orbits of the grains are usually assumed. First, it results in the constancy of ambient plasma parameters along such orbits. Second, it makes the grain's velocity relative to the bulk of plasma independent of time. Thus the potential of such a grain does not depend on time and is determined solely by the radius of its orbit. The fact that the real dust grains can move along eccentric paths is ignored in most papers. However, the eccentric orbits (i) allow grains to penetrate different plasma environments and (ii) introduce periodic variations of the grain's velocity relative to the bulk of plasma.

In what follows, we will represent the variable potential of the grain moving along an eccentric orbit by a function of distance, $\varphi = \varphi(r)$, where $\varphi(r)$ is the solution of the balance Eq. (1) at the distance r from the planet. However, we will assume that φ does not depend on time explicitly. To justify this assumption, consider the time variation of the potential, determined by the equation

$$\frac{{\rm d}\varphi}{{\rm dt}} = \sum_i j_i(r, \varphi), \qquad (2)$$

where $j_i(r, \varphi)$ are the rates of the grain's potential variations at the distance r from the planet due to a number of processes of charge exchange between the grain and environment (cf. (1)). The weak dependence of the rates on the grain's velocity relative to the bulk of plasma was reported by Horányi et al. (1992) and is ignored in (2). Usually j_i are proportional to the ambient plasma density. (The exception is the photoelectron emission which is relatively small near Saturn.) Thus, when the plasma density increases, the rate of the grain's potential variation becomes high and the equilibrium potential $\varphi = \varphi(r)$ such that $\sum j_i(r, \varphi(r)) = 0$ is reached soon. Indeed, a dust grain of size $s = 1\,\mu$m with the potential ≈ -5 V, a value close to that favoured by most authors for a grain in the vicinity of Enceladus, carries ≈ 3500 extra electrons on its surface. The number density of thermal electrons near the orbit of Enceladus is $n \approx 90$ cm^{-3}. Their temperature (about 3 K) corresponds to the thermal speed $u = 9.5$ km sec^{-1}. Simple calculation gives the rate of collisions of thermal electrons with the grain $\sim \pi s^2 n u \approx 2.5$ events per second. The amount of extra electrons necessary to develop the potential -5 V is thus collected during ~ 20 minutes or 10^{-2} times the grain's orbital period. This means that the grain's potential responds to changes of the plasma parameters very quickly.

The case of low plasma density is discussed in (Burns & Schaffer 1989). When the orbital anomaly phase lag of the grain's potential becomes large, the Lorentz force is able to spread grains in space due to both semimajor axis and eccentricity variations. This is the case for so-called resonant charge variations. However, this is not the case for Saturn, where plasma is dense enough to reduce the phase lag to small values which we can safely neglect.

2.2. A supplement to the Hamilton–Krivov integral of the motion

Hamilton & Krivov (1996) developed the analytical theory for the investigation of the circumplanetary dust dynamics. The authors assumed that the grain's orbital plane, planet's equatorial plane and the planet's orbital plane all coincide. Then the orbit-averaged equations of motion under the radiation pressure, planetary oblateness (the coefficient J_2 of the multipole expansion of the gravitational potential) and the Lorentz force in the case of constant charge take the form (the solar tidal term is not considered in this paper)

$$\frac{\mathrm{d}\phi_\odot}{\mathrm{d}\lambda_\odot} = C\frac{\sqrt{1-e^2}}{e}\cos\phi_\odot + \frac{W}{(1-e^2)^2} + \frac{L}{(1-e^2)^{3/2}} - 1, \quad (3)$$

$$\frac{\mathrm{d}e}{\mathrm{d}\lambda_\odot} = C\sqrt{1-e^2}\sin\phi_\odot, \quad (4)$$

where $\phi_\odot$ is the angle between the directions from Saturn to the Sun and to the pericenter of the orbit (solar angle), e is the orbital eccentricity, $\lambda_\odot$ is the solar longitude which substitutes time in the equations of the motion. Note that the equations are written in the reference frame synchronously rotating with the Sun around the planet. This is the reason for the '-1' term in the first equation. The perturbation parameters are defined as

$$C = \frac{9}{8}\frac{n}{n_\odot}Q_{\rm pr}\frac{F_\odot a^2}{\kappa^2 c\rho s} \quad (5)$$

$$W = \frac{3}{2}J_2\left(\frac{R_{\rm p}}{a}\right)^2\frac{n}{n_\odot} \quad (6)$$

$$L = 2\frac{n}{n_\odot}\frac{n}{\Omega_{\rm p}}\frac{q_0 B_0 R_{\rm p}^3\Omega_{\rm p}}{\kappa^2 cm} \quad (7)$$

for the radiation pressure, planetary oblateness and the Lorentz force in the case of constant charge, respectively. Here n and $n_\odot$ are the mean motions of the grain and the Sun, a is the semimajor axis of the grain's orbit, s, m and $\rho = 1\,\mathrm{g\,cm^{-3}}$ are the radius, mass and the density of the grain assumed to be an ice ball, $Q_{\rm pr}$ is the radiation efficiency factor (assumed to equal unity), $F_\odot$ is the flux of radiation energy at the heliocenteric distance of Saturn, $\kappa^2 = 3.79\times10^{22}\,\mathrm{cm^3\,sec^{-2}}$, $R_{\rm p} = 60330\,\mathrm{km}$ and $\Omega_{\rm p} = 1.69\times10^{-4}\mathrm{sec^{-1}}$ are the gravitational parameter, equatorial radius and the magnitude of the planet's spin vector, c is the speed of light. The Lorentz force depends on the grain's charge q_0 and the induction of the planetary magnetic field assumed to match that of a dipole and to equal $B_0 = 0.2154\,\mathrm{G}$ at the Saturnian equator.

Hamilton & Krivov showed that Eqs. (3)–(4) are semicanonical with the "Hamiltonian"

$$\mathcal{H}_0 = \sqrt{1-e^2} + Ce\cos\phi_\odot + \frac{W}{3(1-e^2)^{3/2}} + \frac{L}{2(1-e^2)} \quad (8)$$

which gives the integral of the motion $\mathcal{H}_0(e,\phi_\odot) = \mathrm{const}$. They used the Hamiltonian formalism to investigate the existence and stability of fixed points. They found that Eqs. (3)–(4) have up to five stationary points, depending on the values of the parameters C, W and L. Two points $P_1 = (0,\pi/2)$ and $P_2 = (0,3\pi/2)$ correspond to one and the same point in the $e\cos\phi_\odot$–$e\sin\phi_\odot$ space. These stationary points are not fixed points of (3)–(4). However, they are physically meaningful: radiation pressure causes orbits with very tiny eccentricities to precess or regress rapidly away from P_2 toward P_1. The other three points are shown on the upper left panel in Fig. 2. The plot gives an example of how the stationary points determine the appearance of trajectories in phase space. The detailed analysis of topology of phase portraits is given in (Hamilton & Krivov 1996).

Now let us generalize the foregoing approach to a variable grain's charge $q(r)$. One can easily expand it to the series in r/a

$$q(r) = \sum_{k=0}^{\infty} q_k\left(\frac{r}{a}\right)^k, \quad (9)$$

where q_k are constants. The Lorentz force in the magnetic field $\boldsymbol{B}$ acting on a grain which moves at the distance $\boldsymbol{r}$ with the velocity $\boldsymbol{v}$ in the planetocentric reference frame

$$\boldsymbol{F}_{\rm L} = qc^{-1}\,(\boldsymbol{v} - \boldsymbol{\Omega}_{\rm p}\times\boldsymbol{r})\times\boldsymbol{B} \quad (10)$$

after substitution of (9) takes the form of the series

$$\boldsymbol{F}_{\rm L} = \sum_{k=0}^{\infty} q_k\left(\frac{r}{a}\right)^k c^{-1}(\boldsymbol{v} - \boldsymbol{\Omega}_{\rm p}\times\boldsymbol{r})\times\boldsymbol{B} \quad (11)$$

On the base of the latter equation, the orbit-averaged equations of the motion can be obtained for the Lorentz force in the case of a distance-dependent charge

$$\left\langle\frac{\mathrm{d}\phi_\odot}{\mathrm{d}\lambda_\odot}\right\rangle_{\rm L} = \sum_{k=0}^{\infty} R_k^{(\phi)}(e,\phi_\odot), \quad (12)$$

$$\left\langle\frac{\mathrm{d}e}{\mathrm{d}\lambda_\odot}\right\rangle_{\rm L} = \sum_{k=0}^{\infty} R_k^{(e)}(e,\phi_\odot) \quad (13)$$

In accordance with (Burns & Schaffer 1989) for all integer k (not only positive) one gets $R_k^{(e)} = 0$. Therefore, acting alone, the Lorentz force due to a constant or distance-dependent charge causes precession or regression of the solar angle but does not alter the eccentricity. As follows from Eqs. (3)–(4), it is only the radiation pressure which binds together the evolution of the eccentricity and the behavior of the solar angle. Note, however, that in a general three-dimensional problem the Lorentz force due to variable charge is able to change the eccentricity and the semimajor axis of the grain's orbit as well.

In practice the linear approximation for the function $q(r)$ can be used instead of the infinite series (9) and the functions $R_k^{(\phi)}$ can be expanded in powers of eccentricity. Table 1 shows several first terms of such expansion ($k = 0\ldots4$) together with the errors introduced by ignoring the higher-order terms. It is easy to see that for $k = 0$ the residuals grow rapidly enough with the eccentricity that makes it impossible to use the truncated $R_0^{(\phi)}$-series. Fortunately, $R_0^{(\phi)}$ is relatively simple and have already

Table 1. Approximate right-hand sides of the equations of the motion accounting for the charge variations and their residuals for $\Omega_\mathrm{p}/n = 3.2$ (the ratio of the angular velocity of Saturn's rotation to the mean motion of Enceladus).

k	$V_k = R_k^{(\phi)}(0,\phi_\odot)$	$R_k^{(\phi)}(e,\phi_\odot) - V_k$		
		e=0.2	e=0.4	e=0.6
1	$\frac{1}{2}\frac{q_1 B_0 R_p^3}{a^3 cm}\left[\frac{\Omega_p}{n}+3\right] n_\odot^{-1}$	0.64%	2.9%	8.0%
2	$\frac{q_2 B_0 R_p^3}{a^3 cm}\left[\frac{\Omega_p}{n}+1\right] n_\odot^{-1}$	1.6%	6.8%	18%
3	$\frac{1}{2}\frac{q_3 B_0 R_p^3}{a^3 cm}\left[3\frac{\Omega_p}{n}+1\right] n_\odot^{-1}$	1.9%	8.2%	23%
4	$2\frac{q_4 B_0 R_p^3}{a^3 cm}\frac{\Omega_p}{n} n_\odot^{-1}$	0.64%	2.9%	8.0%
0	$2\frac{q_0 B_0 R_p^3}{a^3 cm} n_\odot^{-1} = L$	6.0%	24%	49%

been analyzed in (Hamilton & Krivov 1996). Replacement of the $R_k^{(\phi)}$ for $k = 1\ldots4$ with the first terms of the relevant expansions leads to reasonably small residuals for eccentricities up to 0.6 and can be used instead of awkward precise expressions.

To account for the charge variability, Eqs. (3)–(4) are therefore extended to

$$\frac{\mathrm{d}\phi_\odot}{\mathrm{d}\lambda_\odot} = C\frac{\sqrt{1-e^2}}{e}\cos\phi_\odot + \frac{W}{(1-e^2)^2} + \frac{L}{(1-e^2)^{3/2}} + V - 1, \quad (14)$$

$$\frac{\mathrm{d}e}{\mathrm{d}\lambda_\odot} = C\sqrt{1-e^2}\sin\phi_\odot, \quad (15)$$

where $V = \sum V_k$ is the term due to the variable charge, and $V_k = R_k^{(\phi)}(0,\phi_\odot) = R_k^{(\phi)}(0)$. Eqs. (14)–(15) have the integral of the motion

$$\mathcal{H} = (1-V)\sqrt{1-e^2} + Ce\cos\phi_\odot + \frac{W}{3(1-e^2)^{3/2}} + \frac{L}{2(1-e^2)}. \quad (16)$$

It is easy to see that introducing the variable charge which depends only on the distance from the planet does not complicate the integral of (Hamilton & Krivov 1996). Indeed, adjusting the coefficients $C' = C\,\mathrm{sgn}(1-V)/(1-V)$, $W' = W\,\mathrm{sgn}(1-V)/(1-V)$, $L' = L\,\mathrm{sgn}(1-V)/(1-V)$, or performing multiplication of the Hamiltonian $\mathcal{H}$ by the $\mathrm{sgn}(1-V)/(1-V)$ – the operation which does not affect the curves $\mathcal{H} = \mathrm{const}$ – we reduce the new integral (16) to Eq. (8). It is clear that the sign of each primed coefficient matches the sign of the non-primed one. However, the term $\mathrm{sgn}(1-V)\sqrt{1-e^2}$ can now be either positive or negative, depending on the sign of $1-V$.

The case of a positive sign ($V = 0$, $1-V = 1 > 0$) is carefully analyzed in (Hamilton & Krivov 1996). In the case of opposite sign there are specific combinations of parameters when the phase portrait can be mirrored against the $e\cos\phi_\odot = 0$ axis. This case is demonstrated by the second row of plots in Fig. 2. Note that the case of negative sign can be interpreted as the backward motion of the Sun.

Table 2. Numerical values of the parameters C, W, L, and $V = V_1$ for various charging models. The grain size s is in microns.

Charging model	$L \cdot s^2$	$V \cdot s^2$	W	$C \cdot s$
Constant -5.6 V	-15.45	0	12.61	0.6575
Jurac et al. (1995)	-37	33		
Morfill et al. (1993)	-10	-123		
Horányi et al. (1992)	-14	-49		

2.3. Dynamics for different charge models

With the grain's potentials $\varphi(r)$ shown in Fig. 1 and using the integral (16) the phase portraits of the motion (the curves $\mathcal{H} = \mathrm{const}$) were built for several E ring dust charging models (Fig. 2). In order to obtain the phase portraits, the potentials were approximated by linear functions of the distance in the neighbourhood of the orbit of Enceladus. The corresponding values of L and V are given in Table 2, as well as the values of C and W shared by all charging models.

Fig. 2 also presents the numerical solutions of the full Newtonian equations of the motion $\boldsymbol{F} = m\ddot{\boldsymbol{r}}$, taking into account the planetary obliquity and non-zero grain's orbital inclinations. In these numerical integrations, the potentials were calculated by linear interpolation, using the voltage values sampled by $0.5R_\mathrm{p}$. Shown in the figure are the phase trajectories for the grains initially in circular orbits. Despite many simplifications used to derive Eqs. (14)–(15), the numerical and analytical results are in fairly good agreement.

Variation of the charging model parameters (i.e. the function $q(r)$) leads to variation of the grain's radius s_m, for which the maximum orbital eccentricity, developed by an initially circular orbit, is the largest. The value of this largest eccentricity depends on the charging model as well (Fig. 3).

The difference between the phase portraits for different charging models gives rise to the question: which charge models are consistent (provided that the dynamical model is correct) with the large radial extent and narrow size distribution of the ring derived from observations? Let us check which charging models are suitable in this sense, i.e. allow the grains with radii $s \in [0.3\,\mu\mathrm{m}, 3\,\mu\mathrm{m}]$ (Nicholson et al. 1996) to attain large orbital eccentricities for the problem under consideration (radiation pressure + planetary oblateness + Lorentz force + variable charge).

As seen from the obtained solutions, suitable models are the constant charge and the variable charge of Jurac et al. (1995). They allow grains of radii $\approx 1\,\mu$m to develop large eccentricities ($\max e > 0.5$). The charge given by Horányi et al. (1992) evaluated for $\delta_\mathrm{m} = 1.0$ is less compatible with the observational data on the E ring since it gives too low maximum eccentricity for the grains of $s = 1.6\,\mu$m. Indeed, Horányi et al. (1992) reject this model and choose another one for $\delta_\mathrm{m} = 1.5$ which gives almost constant charge $\varphi = -5.6$ V. The least suitable model

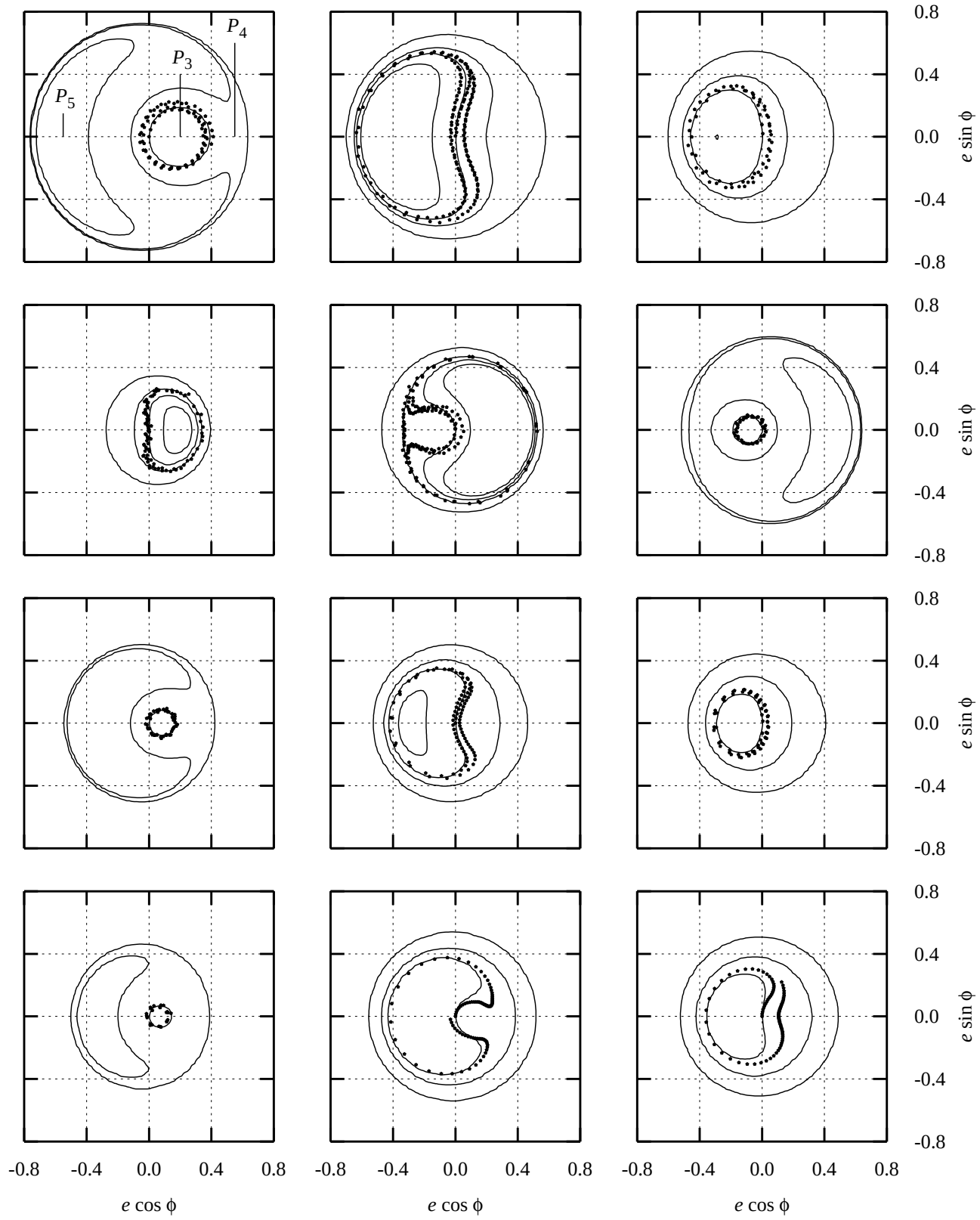

Fig. 2. Phase portraits of the motion of the grains with variable potential $\varphi = \varphi(r)$ in Saturn's magnetic field with account for the radiation pressure, planetary oblateness and the Lorentz force. Top to bottom: constant charge -5.6 V (left to right: $s = 1\,\mu$m, 1.1 μm, 1.2 μm); charge of Jurac et al. (1995) (0.6 μm, 0.85 μm, 1 μm); charge of Horányi et al. (1992) (1.4 μm, 1.6 μm, 1.8 μm); charge of Morfill et al. (1993) (3.0 μm, 3.15 μm, 3.3 μm). The numerical solution of Newton's equations of the motion $\boldsymbol{F} = m\ddot{\boldsymbol{r}}$ with the initial data $e = 0$ is overplotted with dots.

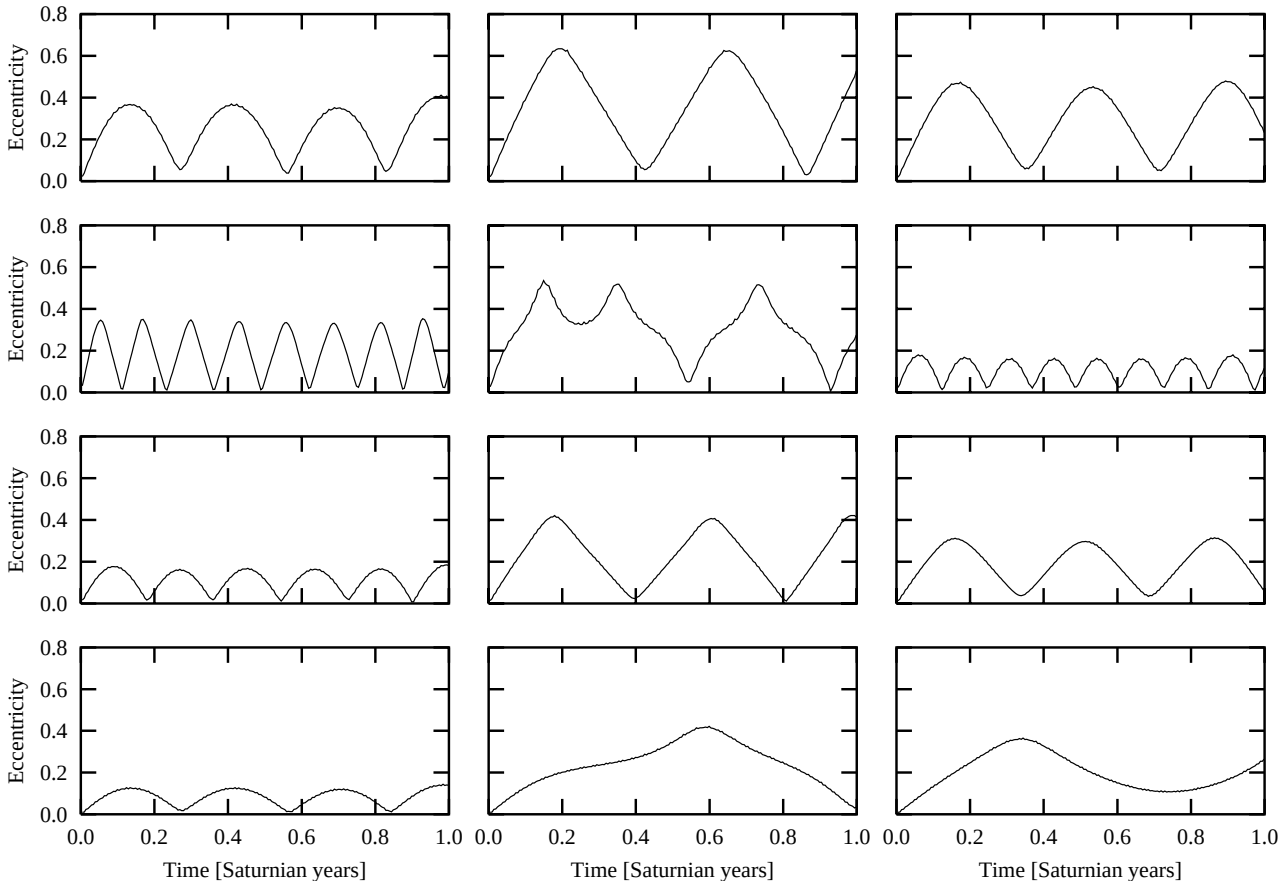

Fig. 3. Evolution of eccentricity for an initially circular orbit. The sizes and the charging models are the same as those in Fig. 2. The data were obtained from the numerical solution of Newton's equations of the motion.

is one favoured by Morfill et al. (1993) who used a different dynamical model accounting for the plasma drag only. In our dynamical model their potential allows attaining considerable orbital eccentricities for the grains of $s = 3.2$, i.e. outside the interval $[0.3\,\mu\mathrm{m}, 3\,\mu\mathrm{m}]$.

3. The plasma drag

3.1. Calculation of the plasma drag force

Saturn's magnetosphere co-rotates with the planet with the angular velocity Ω_p. At the distance of Enceladus from Saturn the linear speed of a dust grain on the circular Keplerian orbit is 3.2 times less than that of the plasma particles picked up by the planetary magnetic field. Thus E ring dust is accelerated by the plasma.

To make numerical estimates of the plasma effect on a grain we use Saturn's plasma model of Richardson (1995). The number density of charged particles over a range of distances from Saturn is reproduced in Fig. 4a. The most abundant in the inner magnetosphere is the fraction of the "cold" (thermal) electrons. They are followed by the heavy ions, supposedly the combinations of water group ions (O^+, OH^+, H_2O^+, H_3O^+) and N^+ ones which have the atomic number about 16. The much less dense fraction of Saturn's magnetosphere is that of the hydrogen ions (protons) and the least dense one is composed of the "hot" (suprathermal) electrons, the number density of which does not exceed 0.4 cm^{-3} and is not presented in the graph. Calculation of the mass density (number density times particle's mass) shows the dominance (up to 2 orders of magnitude, see Fig. 4d) of the heavy ion fraction.

Striking contrast of the spatial densities suggests that the interaction of dust grains with some of the fractions can be safely neglected. In order to estimate the drag force due to each fraction, we represent the motion of the grain around Saturn by a circular Keplerian orbit and calculate the direct drag forces (Banaszkiewicz et al. 1994)

$$F_\mathrm{D} = \pi n_i m_i u_i^2 s^2 \left[\left(M_i + \frac{1}{2M_i} \right) \frac{\exp(-M_i^2)}{\sqrt{\pi}} + \left(M_i^2 + 1 - \frac{1}{4M_i^2} \right) \mathrm{erf}(M_i) \right] \qquad (17)$$

and the Coulomb drag forces (Northrop & Birmingham 1990)

$$F_\mathrm{C} = \frac{\sqrt{\pi} q^2 e^2 n_i}{m_i v^2} \int_{-\infty}^{+\infty} \frac{y}{|y|^3} \left(2M_i y - 1\right) \times \exp\left[-(y - M_i)^2\right] \ln \frac{1 + (m_i u_i^2 \lambda_\mathrm{D} y^2/(qe))^2}{1 + (m_i u_i^2 s y^2/(qe))^2} \, dy \qquad (18)$$

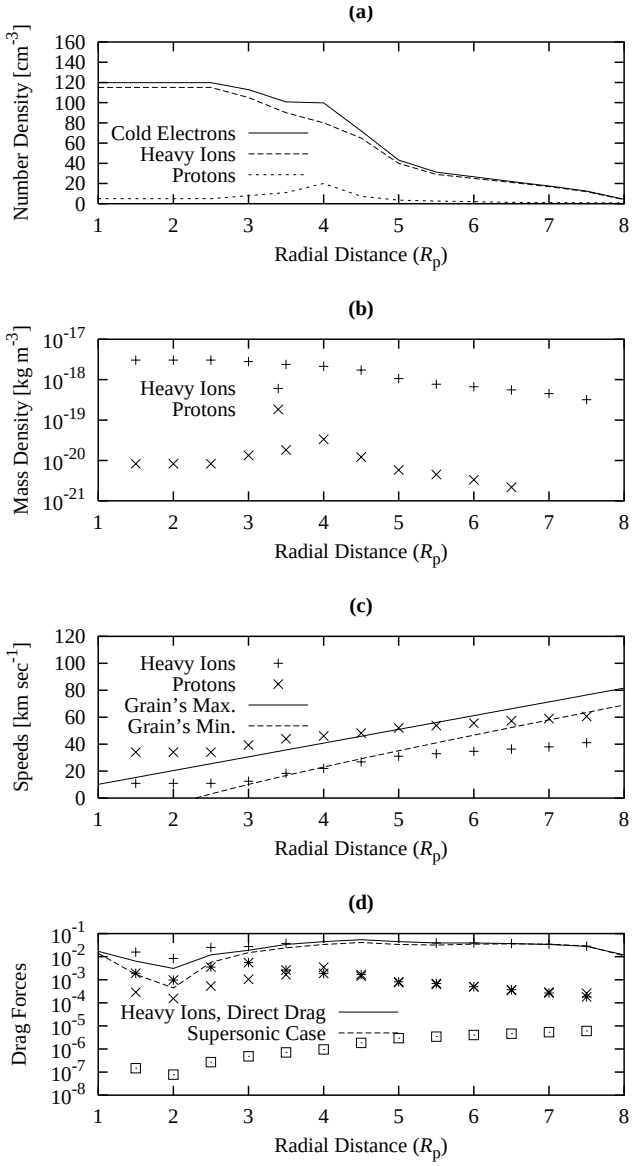

Fig. 4a–d. Saturn's plasma and its effect on the motion of the E ring grains: (a) number density of the charged particles versus distance from Saturn (hot electrons are not shown), (b) mass density, (c) the grain speed relative to the bulk of plasma (shown are the maximum and minimum values for a grain on a Keplerian orbit) and the thermal speed of ions, (d) plasma drag force due to various fractions in the units of the solar radiation pressure (vertical crosses are heavy ions, diagonal crosses are protons, "bugs" are cold electrons, bars are hot electrons, solid line is the plasma drag force due to direct collisions with the heavy ions, and the dashed line is the same force in supersonic approximation.

for each fraction i, determined by the number density n_i and thermal speed u_i of the charged particles of mass m_i. A grain is defined by its radius s, charge q (assumed to be -5.6 V) and the velocity v relative to the bulk of plasma. The latter allow us to calculate the Mach number $M_i = v/u_i$. Note that in (18) e temporarily denotes the elementary charge (CGS units). Symbol $\lambda_{\rm D}$ stands for the minimum Debye length $\sqrt{kT_i/4\pi n_i e^2}$ among all the fractions. For Saturn's inner magnetosphere it is the one of the thermal electrons which ranges from 70 cm at the distance $3R_{\rm p}$ to 12 m at $8R_{\rm p}$.

Fig. 4d presents estimates of the plasma drag forces due to various fractions. Heavy ions dominate all other fractions. The solid line shows the drag force due to direct collisions of the heavy ions with the grain, i.e. without Coulomb drag. It is easy to see that the Coulomb drag gives negligible contribution to the plasma drag force. Thus when evaluating the plasma drag force it is necessary and sufficient to account for the direct drag due to heavy ions.

The E ring dust grains move with the supersonic speed with respect to the heavy ion fraction (see Fig. 4c). In this case $F_{\rm C}/F_{\rm D} \to 0$ (Morfill & Grün 1979) and the sophisticated expression (17) can be replaced with its $M_{\rm H} \to \infty$ asymptotic

$$F_{\rm D} = \pi n_{\rm H} m_{\rm H} s^2 v^2. \tag{19}$$

The value of the direct drag evaluated with (19) is given in the Fig. 4d (dashed line).

3.2. The main features of the planar motion

In the E ring region the plasma drag force is at least 15 times weaker than the radiation pressure (Fig. 4d). Therefore, if an orbital element is perturbed by the radiation pressure or a like-strength force, the plasma drag is unimportant. This is the case for the eccentricity and the solar angle, which are subject to changes by the three forces discussed in Sect. 2. In contrast, the semimajor axis is perturbed neither by the radiation pressure, planetary oblateness nor the Lorentz force, but it experiences a secular perturbation due to the plasma drag. The growth of the semimajor axis is especially interesting since apart from the spreading dust in space it leads to remarkable effects in the elements e, $\phi_\odot$.

The perturbation of the semimajor axis of the grain's circular orbit ($e = 0$) due to the plasma drag force (19) is

$$\frac{{\rm d}a}{{\rm d}\lambda_\odot} = \frac{3}{2}\, a\, \frac{a}{s}\, \frac{\rho_{\rm H}}{\rho}\, \frac{|\Omega_{\rm p} - n|}{n_\odot}\, \left(\frac{\Omega_{\rm p}}{n} - 1\right). \tag{20}$$

The semimajor axis of a micron-sized grain launched from Enceladus increases by ≈30% after one planetary year. (This value is obtained using (17).) The growth of the semimajor axis makes the parameters C, W, L, V dependent on time.

Rewrite Eqs. (14)–(15) using new variables $h = e\cos\phi_\odot$, $k = e\sin\phi_\odot$ and linearize them for small eccentricities (around $h = k = 0$). We have

$$\frac{{\rm d}h}{{\rm d}\lambda_\odot} \;=\; -\gamma k, \tag{21}$$

$$\frac{{\rm d}k}{{\rm d}\lambda_\odot} \;=\; \gamma h + C, \tag{22}$$

where $\gamma = W + L + V - 1$. For constant γ and C, the solution of (21)–(22) with the initial data $h = k = 0$ is

$$h(\lambda_\odot) \;=\; C\gamma^{-1}(\cos\gamma\lambda_\odot - 1) \tag{23}$$

$$k(\lambda_\odot) \;=\; C\gamma^{-1}\sin\gamma\lambda_\odot. \tag{24}$$

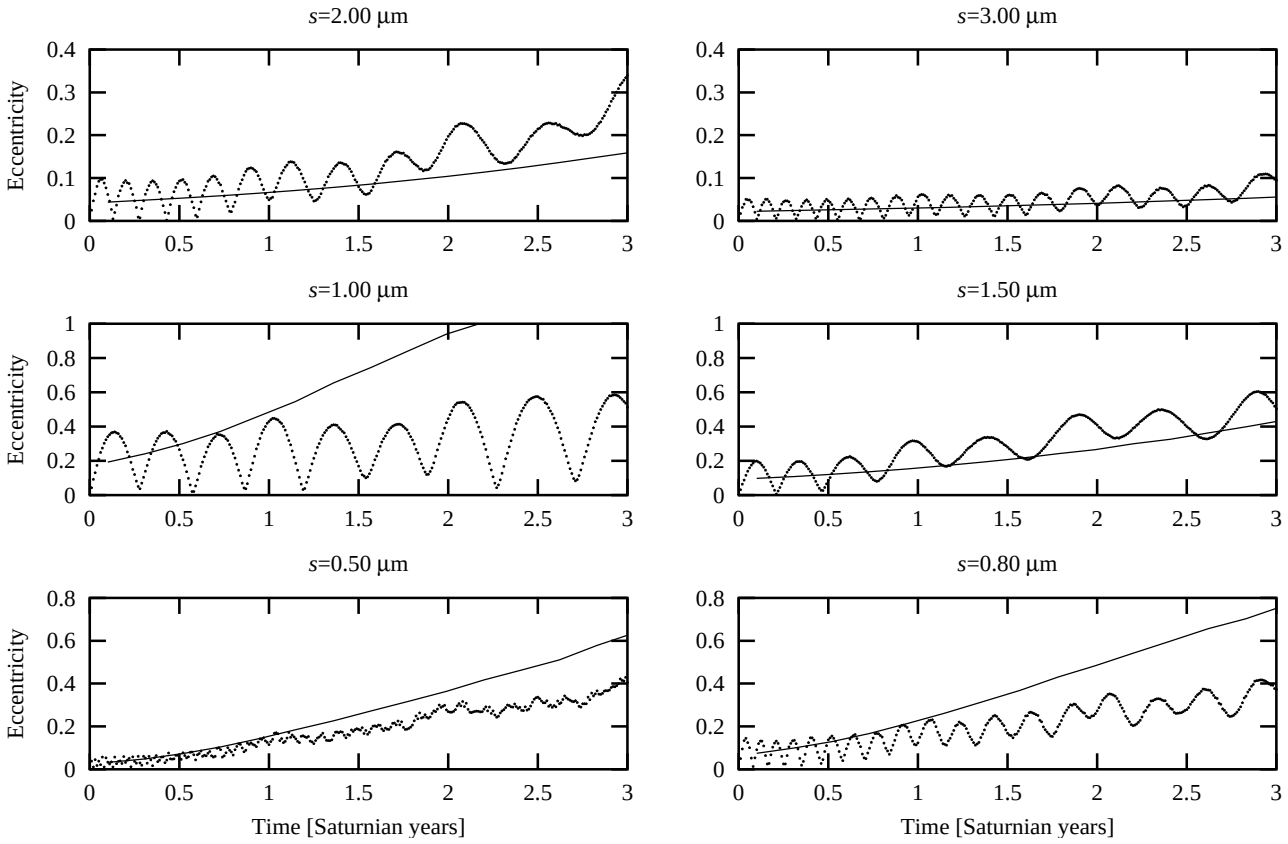

Fig. 5. The evolution of eccentricity ($e = \sqrt{h^2 + k^2}$) for different-sized grains with the constant charge of -5.6 V (dots). Solid line shows $|C\gamma^{-1}|$. Time is measured in Saturnian years.

However, the growth of the semimajor axis makes γ and C functions of time, or equivalently, of $\lambda_\odot$. Assuming linear dependence

$$\gamma(\lambda_\odot) = \gamma(0) + \gamma'(0)\lambda_\odot,$$
$$C(\lambda_\odot) = C(0) + C'(0)\lambda_\odot$$

and inserting these equations into (21)–(22) allows one to obtain the "perturbed" solution in explicit form. This solution is valid for moderate time intervals, until the assumption of small eccentricities is broken. However this analytical solution proves to be quite difficult to interpret and does not make the problem more tractable, hence we choose a different way.

Looking at the numerical solution of the problem one can see that in most cases the trajectories conserve the character of harmonic oscillations but the center of the oscillations drifts in the (h, k) plane. This fact can be reproduced analytically without solving (21)–(22). Indeed, it is easy to find the center of curvature of the solution at the point (h, k):

$$h_\mathrm{c} = h - \frac{h'^2 + k'^2}{h'k'' - h''k'}k',$$
$$k_\mathrm{c} = k + \frac{h'^2 + k'^2}{h'k'' - h''k'}h',$$

where h', k', h'', k'' are derivatives with respect to $\lambda_\odot$ to be substituted from Eqs. (21)–(22). Expansion to Taylor series with respect to the variables h, k up to the terms of the first order gives

$$h_\mathrm{c} = -\frac{C}{\gamma} + \frac{C\gamma' - \gamma C'}{\gamma^2 C}k, \quad (25)$$
$$k_\mathrm{c} = 0. \quad (26)$$

As the second term in (25) is small, it is evident that the solution rotates about the center $(-C(\lambda_\odot)/\gamma(\lambda_\odot),\ 0)$. Fig. 5 shows the evolution of the eccentricity $e = \sqrt{h^2 + k^2}$ for the grains of various sizes in the case of a constant potential. The solid line presents $|C\gamma^{-1}|$. Until the eccentricity gets large, $|C\gamma^{-1}|$ traces the instantaneous center of the oscillations for all grain sizes except for a narrow interval around s such that γ is close to zero and the assumption of small eccentricities is broken very soon.

Note that neglecting the planetary oblateness and the Lorentz force still does not stop the drift of the center of the oscillation. Indeed, $W = L = V = 0$ means $\gamma = -1 = \mathrm{const}$ whereas C remains a function of time due to the growth of the semimajor axis. This is the case for the Hyperion dust discussed by Banaszkiewicz & Krivov (1997).

3.3. Radial drift of the E ring dust

The growth of the semimajor axis of the grain orbits due to the plasma drag is responsible for remarkable transportation of dust launched from Enceladus outward from Saturn. With the plasma parameters of Richardson's (1995) model, the growth rate of the

semimajor axis of a grain launched from Enceladus is estimated to be $0.30/s$ times the initial value per planetary year, where s is measured in microns. This rate is large enough to contribute considerably to the formation of the E ring structure (Dikarev & Krivov 1998).

The growth rate of the semimajor axis decreases with the increasing grain radius s. Thus the orbital evolution of large grains can be described in terms of the "radiation pressure + planetary oblateness" model. (The Lorentz force decreases $\propto s^{-2}$ and does not play an important role for large grains either.) The planetary oblateness causes quick precession of the orbit which does not permit the radiation pressure to develop large eccentricities. These grains orbit Saturn close to Enceladus and collide with the satellite in short time (Horányi et al. 1992). This mechanism explains the absence of large grains ($s \gg 1\,\mu$m) in the E ring.

When the grain radius decreases the Lorentz force comes into play. It causes the orbital regression which cancels out the orbital precession due to the planetary oblateness roughly at $s = 1\,\mu$m. The radiation pressure sends the grains to highly eccentric orbits which allow them to avoid recollision with the satellite for a long time.

According to Horányi et al. (1992) the orbits of the grains with $s < 1\,\mu$m quickly regress due to the Lorentz force which does not permit the radiation pressure to introduce large eccentricities. This was thought to be the explanation for the absence of small dust grains ($s \ll 1\,\mu$m) in the E ring. Inclusion of the plasma drag force necessitates corrections to this model regarding the small grains. Indeed, the amplitude of the eccentricity oscillations $\sim C/\gamma \propto s$ decreases proportional to the radius of the grains, the motion of which is dominated by the Lorentz force. Decrease of the amplitude narrows the recollision zone (i.e. the range of a when the grain's orbit intersects that of the satellite). The rate of growth of the semimajor axis is $\propto s^{-1}$, so that a decrease of the grain radius decreases the period of stay in the zone.

Special computations show that almost all submicron particles avoid recollision with Enceladus and spread in space beyond its orbit. They can be eliminated later due to collision with other satellites, sputtering and mutual collisions. The most rapidly drifting grains ($s \approx 0.1\,\mu$m), which are still within the applicability limits of the orbit-averaging technique, can cross the ring as fast in ~ 0.5 planetary year.

Finally, the tiniest dust grains of radii $s \ll 0.1\,\mu$m are small enough to let the planetary magnetic field pick them up and accelerate to the co-rotational speed. They do not leave the neighbourhood of Enceladus' orbit but move several times faster than the parent moon and should reimpact it very soon.

4. Conclusions

This paper deals with Saturn's E ring dust grain dynamics. First, it extends the analytical theory of the circumplanetary dust dynamics by Hamilton & Krivov (1996). In order to account for the grain's charge variability, a reasonable approximation of the potential depending on the distance from the planet is suggested and its effects are considered when combined with the solar radiation pressure, planetary oblateness and the Lorentz force due to dipole magnetic field. It is found that the distance-dependent charge does not alter the eccentricity but causes precession or regression of the orbit with the rate depending on the charging model. The variable charge does not extend the set of the phase portrait topologies described by Hamilton & Krivov (1996). Like the constant charge, the variable one allows orbits to attain large eccentricities, with the charging model by Jurac et al. (1995) being a reasonable alternative to that of Horányi et al. (1992).

Second, the action of the plasma drag is investigated analytically in the approximation of small eccentricities and zero inclinations. On the base of the plasma model for Saturn (Richardson 1995) it is shown that direct drag due to the heavy ion fraction (usually referred to as the oxygen ions) is the only drag force component which is necessary to account for. Grain's interactions with other fractions and the Coulomb drag due to the heavy ions can also be ignored in the plasma drag model. The primary effect of the plasma drag on a grain's orbit is the gradual growth of the semimajor axis. This in turn leads to the long-term growth of the eccentricity when the drag is introduced simultaneously with the radiation pressure. The rate of the semimajor axis growth is rapid enough to let the submicron grains launched from Enceladus on the circular orbit leave the sweeping zone and thus escape from recollision with the parent satellite.

Acknowledgements. The author is greatly indebted to Dr. A.V. Krivov for useful discussions and advice. Thanks are also due to Dr. H. Krüger for his assistance in evaluating this paper. The work was supported by a grant for young scientists of St. Petersburg in 1997, 1998.

References

Acuña M.H., Connerney J.E.P., Ness N.F., 1983, J. Geophys. Res. 88, 8771
Banaszkiewicz M., Krivov A.V., 1997, Icarus 129, 289
Banaszkiewicz M., Fahr H.J., Scherer K., 1994, Icarus 107, 358
Burns J.A., Schaffer L., 1989, Nat 337, 340
Dikarev V.V., Krivov A.V., 1998, Solar System Res. 32(2), 128
Hamilton D.P., Krivov A.V., 1996, Icarus 123, 503
Horányi M., Burns J.A., Hamilton D.P., 1992, Icarus 97, 248
Jurac S., Baragiola R.A., Johnson R.E., Sittler E.C. Jr., 1995, J. Geophys. Res. 100, 14821
Morfill G.E., Grün E., 1979, Planet. Space Sci. 27, 1269
Morfill G.E., Havnes O., Goertz C.K., 1993, J. Geophys. Res. 98, 11285
Nicholson P.D., Showalter M.R., Dones L., et al., 1996, Sci 272, 509
Northrop T.G., Birmingham T.J., 1990, Planet. Space Sci. 38, 319
Richardson J.D., 1995, Geophys. Res. Lett. 22, 1177